International Journal of Applied Ceramic Technology

Submitted April 26th, 2018

Accepted July 2nd, 2018

Characterization of vacuum-annealed $TiNb_2O_7$ as high potential anode material for lithium-ion battery

Ryoji Inada*, Tomoya Mori, Rei Kumasaka, Ryuta Ito, Tomohiro Tojo, and Yoji Sakurai

Department of Electrical and Electronic Information Engineering,

Toyohashi University of Technology,

1-1 Hibarigaoka, Tempaku-cho, Toyohashi, Aichi 441-8580, Japan.

*Corresponding author

Ryoji Inada, Associate Professor

Postal address: Toyohashi University of Technology, 1-1 Tempaku-cho, Toyohashi,

Aichi 441-8580, Japan

Phone: +81-532-44-6723

Fax: +81-532-44-6757

E-mail address: inada@ee.tut.ac.jp

ORCID ID: 0000-0002-6357-092X

ABSTRACT

Electrochemical properties of mixed titanium-niobium oxide $TiNb_2O_7$ (TNO) synthesized via vacuum annealing as high potential anode material for lithium-ion batteries were investigated. Crystal structure, size and morphology are nearly independent of the annealing atmosphere for starting materials but the color of vacuum-annealed TNO (TNO-V) is dark blue while white for the air-annealed one (TNO-A). X-ray photoelectron spectroscopy analysis also indicated that Ti^{4+} and Nb^{5+} in TNO are partially reduced into Ti^{3+} and Nb^{4+} due to the introduction of oxygen vacancy. Electronic conductivity for TNO-V was around 10^{-3} S cm^{-1} at room temperature and much higher than that for TNO-A (= 10^{-11} S cm^{-1}). In electrochemical testing, both TNO-A and TNO-V electrodes showed reversible capacity of 260–270 mAh g^{-1} at low current density of 0.5 mA cm^{-2}, while at higher current density of 5.0 mA cm^{-2}, TNO-V electrode retained higher reversible capacity of 140 mAh g^{-1} than that for TNO-A electrode (= 80 mAh g^{-1}). The enhancement of intrinsic electronic conductivity greatly contributes to improve the rate performance of TNO.

Keywords: $TiNb_2O_7$, lithium-ion battery, anode material, oxygen vacancy, electronic conductivity

1. INTRODUCTION

Rechargeable lithium-ion batteries (LiB) have been used as power sources for various electronic devices, such as mobile phones and laptop computers. As an anode material for present LiB, graphite has been commonly used because of its low cost, acceptable storage capacity (= 372 mAh g^{-1}) and stable cycling performance. However, the passivating solid electrolyte interphase (SEI) formed on graphite electrode in the initial charging process via decomposition of organic liquid electrolyte. Moreover, the low Li^+ storage potential of graphite raises safety issues: when charged at high current rate or overcharged, there is possible lithium plating or formation of lithium dendrites and the short circuit in LiB to fire the flammable electrolyte. Safety concern has become the critical issue for large scale applications of LiB, such as hybrid electric vehicles and energy storage system.[1–3]

In order to overcome this problem, titanium-based oxides have attracted wide attention because of relatively high redox potential between 1.0 and 2.0 V vs. Li/Li^+, which avoids the possibility of lithium plating during the charging process.[4–18] Particularly, the zero-strain $Li_4Ti_5O_{12}$ (LTO) with cubic spinel structure was commercialized as a highly safe anode material for LiBs due to its excellent cycle stability and high rate capability.[4–10] However, theoretical Li^+ storage capacity of LTO is limited to 175 mAh g^{-1}, so that development of anode materials with both high safety and high Li^+ storage capacity is strongly required to increase energy density of LiB for large scale applications. Niobium-based oxides with the redox potentials from 1.0 to 2.0 V vs. Li/Li^+ have been also considered as interesting candidates for anode material of LiB with high safety, because it is possible to realize two-electron transfer per niobium by redox couple of Nb^{5+}/Nb^{4+} and Nb^{4+}/Nb^{3+}, resulting into high Li^+ storage capacity. Moreover, these

oxides are nontoxic and more importantly, their redox potential should avoid possible lithium plating. To date, the electrochemical properties for various niobium-based oxides have been reported.[19–42] Among them, mixed titanium-niobium oxides $TiNb_2O_7$, $Ti_2Nb_{10}O_{29}$ and $TiNb_{24}O_{62}$ have high theoretical capacity around 390–400 mAh g^{-1} due to $Ti^{4+/3+}$, $Nb^{5+/4+}$ and $Nb^{4+/3+}$ redox couples.[26, 32, 36, 41] They have the monoclinic "shear ReO_3 structure" with the space group of $C2/m$, consisting of MO_6 (M = Ti, Nb) octahedra sharing edges and corners.[19, 26, 36, 41] At the potential range above 1.0 V vs. Li/Li^+, they shows the reversible capacity of 250–300 mAh g^{-1} and reasonably good cycle stability.

It has been already reported that the rate capability of $TiNb_2O_7$ was significantly improved by carbon coating,[26, 27] reducing the particle size below 100 nm and controlling the particle morphology.[29–32] The former is effective to increase the extrinsic conductivity of active material while the latter plays a role in Li^+ insertion/deinsertion kinetics, by increasing the reaction interface between the active materials and liquid electrolyte and facilitating transport owing to shorter or simpler diffusion paths for Li^+ ions. The reforming the intrinsic properties such as electronic conductivity and Li^+ diffusion coefficient by substituting with alien metal ions and/or controlling the composition is another effective method to improve the electrochemical properties of active materials. Although the electronic conduction in composite electrode is achieved by the conductive carbon, improvement of intrinsic electronic conductivity of active material is quite effective to enhance the rate performance because both the electrons and Li+ ions move in active material during charge and discharge reactions, as shown in the literatures.[9–10] Cu^{2+}, Ru^{4+} and Mo^{6+} doping is confirmed to be effective to improve electrochemical performance for $TiNb_2O_7$.[33–35] Cr^{3+} and Nb^{5+} co-doped $Ti_2Nb_{10}O_{29}$ shows mush superior electrochemical performance to non-doped one.[37] In addition, electrochemical properties

of $Ti_2Nb_{10}O_{29}$ can be improved greatly by introducing oxygen vacancy in the crystal structure.[38–40] Oxygen vacancy can be easily introduced in $Ti_2Nb_{10}O_{29}$ crystal by annealing the precursor in vacuum, Ar and N_2 atmospheres and greatly enhance the electronic conductivity.[38–40] Such improvement in electronic conductivity This method is quite simple, and could be applicable for improving electrochemical performance of other mixed Ti-Nb oxide with different Ti and Nb compositions such as $TiNb_2O_7$ and $TiNb_{24}O_{62}$. Moreover, in the point of view for material cost, TNO with lower Nb contents is preferable because the cost of Nb source is more expensive than Ti source.

In this paper, we synthesized both $TiNb_2O_7$ and $TiNb_2O_{7-x}$ via simple solid state reaction by annealing the mixture of TiO_2 and Nb_2O_5 in air and vacuum atmosphere, in order to reform the intrinsic properties. The influence of introduction of oxygen vacancy into crystal structure, particle morphology, electronic conductivity and electrochemical performance for $TiNb_2O_7$ as anode material for LiB was investigated.

2. EXPERIMENTAL

Samples used in this work were synthesized by a conventional solid state reaction method. Stoichiometric amount of anatase TiO_2 (Kojundo Chemical Laboratory Co., Ltd., 99%) and Nb_2O_5 (Kojundo Chemical Laboratory Co., Ltd., 99.9%) were ground and mixed in ethanol by planetary ball-milling (Nagao System, Planet M2-3F) with zirconia balls for 1 h. The mixture was sealed in a vacuum quartz tube with alumina boat and then annealed at 1050°C for 24 h under a pressure of 0.8 Pa using a tube furnace. For comparison, the sample was also prepared by annealing the same starting materials at 1050°C for 24 h in air.

Crystal structure of both TNO annealed in air (TNO-A) and TNO annealed in

vacuum (TNO-V) were evaluated by X-ray diffractometer (MultiFlex, Rigaku) using Cu$K\alpha$ radiation (λ = 0.15418 nm), with measurement angle range 2θ = 5–90° and step interval of 0.01°. For the measurements, small amount of Si powders were mixed with TNO-A or TNO-V as the reference material. Using the X-ray diffraction (XRD) data for both powder samples, lattice parameters were calculated by Rigaku PDXL XRD analysis software. Scanning electron microscope (SEM, VE-8800, KEYENCE) was used to observe the size and the morphology of both TNO-A and TNO-V particles. The chemical states of Ti and Nb for both samples were characterized by using an X-ray photoelectron spectrometer (Quantera SXM, ULVAC-PHI Inc.) with an Al$K\alpha$ X-ray source (1486.6 eV). Thermogravimetric (TG) analysis of both TNO-A and TNO-V was carried out by using differential thermal balance analyzer (Thermo plus EVO II TG-DTA TG8120, RIGAKU) at temperature range from room temperature to 900°C in flowing air with 500 mL/min, to evaluate the introduction of oxygen vacancy in TNO-V.

Electronic conductivity for both TNO-V and TNO-A was evaluated at 20°C by potentiostatic polarization measurement with an applied DC voltage of 1 V, using a Multi Potentiostat (VSP-300, Bio-Logic). During the conductivity measurement, uni-axial pressure of 5×10^3 N was applied to both powder samples put between the pair of SUS316L electrodes with cylindrical shape. For electrochemical characterization of both TNO-A and TNO-V annealed in different atmospheres, two-electrode set-up was used. Firstly, the composite electrodes were fabricated from a 70:25:5 (wt%) mixture of active material (TNO-A or TNO-V), acetylene black (AB) as a conducting additive, and polytetrafluoroethylene (PTFE) as a binder. The mixture was rolled into thin pellets with thickness of 0.5 mm and punched into 8 mm-diameter circular disks. The mass loading and compacted density of active material (TNO-A or TNO-V) in composite electrodes

were 0.062–0.065 g cm^{-2} and 1.24–1.30 g cm^{-3}, respectively. TNO-A or TNO-V pellet is used as working electrode, where as a single lithium foil serve as both counter and reference electrodes. The electrolyte solution was 1 mol $LiPF_6$ in a mixture or ethylene carbonate (EC) and dimethyl carbonate (DMC) with a volume ratio of 1:1 (Kishida Chemical Co., Ltd.). Together with Celgard 3501 as a separator, these components were assembled in a CR2032 coin type cell. The assembly of the cell was carried out in a dry Ar-filled glove box (UN-650FCH, UNICO). The cell was charged and discharged over a voltage range between 1.0 and 2.5 V versus Li/Li^+ electrode at different fixed current density 0.5–5.0 mA cm^{-2} and 25°C using Battery Test System (TOSCAT-3100, Toyo System).

3. RESULTS AND DISCUSSION

Figure 1(a) shows the comparison of XRD patterns for TNO-A (annealed in air) and TNO-V (annealed in vacuum). It is noted that the diffraction peaks from Si, which was mixed with TNO-A or TNO-V as the reference, are removed from the data. All the peaks for both samples are well indexed with the calculated patterns based on structural data for $TiNb_2O_7$ with monoclinic ReO_3 shear structure with the space group of $C2/m$,[26–35] and no other peaks from secondary phases were detected. However, as shown in Figure 1(b), several specific peaks are slightly shifted to smaller angle. It is noted that all diffraction peaks for TNO-V are confirmed to be shifted to smaller angle and the angle shift for each diffraction peak is much larger than the measuring step (= 0.01°), so that the lattice size for TNO-V is expected to be larger than that for TNO-A. The lattice parameters calculated by using XRD data and PDXL software are a = 1.191 nm, b = 0.3810 nm, c = 2.041 nm and β = 120.20° for TNO-A, while a = 1.193 nm, b = 0.3813 nm, c = 2.041 nm and β =

120.42° for TNO-V. These are very close to the data as previously reported but the parameters *a* and *b* for TNO-V are slightly larger than those for TNO-A.[26–35]

Comparison of photos and SEM images of TNO-A and TNO-V are shown in Figure 2. Both the size and morphology of TNO-A and TNO-V particles are nearly identical and the averaged particle size of both samples is confirmed to be around 0.5–2 μm. However, the color is clearly different among the samples. TNO-A annealed in air is white while TNO-V annealed in vacuum is dark blue. Similar color change was reported in $Li_4Ti_5O_{12}$ with the presence of the mixed Ti^{4+}/Ti^{3+} ions for charge compensation by Ta^{5+}, V^{5+}, W^{6+} and Mo^{6+} doping into Ti^{4+} site.[8–11] It has been also reported that partial reduction from Nb^{5+} to Nb^{4+} in Nb-based oxide also causes similar color change from white to dark blue.[42] Furthermore, in our previous work, $Ti_2Nb_{10}O_{29}$ also shows similar color change by introduction of oxygen vacancy, which is attributed to the partial reduction from Ti^{4+} and Nb^{5+} to Ti^{3+} and Nb^{4+} for charge compensation.[38] In this study, the nominal composition ratios of Ti : Nb of TNO-A and TNO-V are expected to be identical (= 1 : 2). Therefore, if partial reduction from Ti^{4+} and/or Nb^{5+} to Ti^{3+} and/or Nb^{4+} was occurred in TNO-V annealed in vacuum, some amount of oxygen vacancy should be introduced in TNO-V.

In order to confirm the introduction of oxygen vacancy in TNO-V, thermogravimetric (TG) analysis of both powder samples was carried out under flowing air. Figure 3 shows the comparison of thermogravimetric (TG) curves for TNO-A and TNO-V. As can be seen, TNO-A shows no weight change in whole measured temperature range, while the weight of TNO-V gradually increase with temperature above 400°C and becomes constant above 700°C. Increase of the weight for TNO-V from the initial state is confirmed to be 0.4% and after the measurement, the color of TNO-V was changed into

white color as well as TNO-A. These results suggest that oxygen vacancy is introduced in TNO-V and increase of the weight for TNO-V in TG analysis is attributed to the vanishing the oxygen vacancy by the oxidation. If Ti and Nb contents in TNO-V were stoichiometric (Ti : Nb = 1 : 2), the oxygen content in TNO-V is estimated to be 6.91. Therefore, Ti^{4+} and/or Nb^{5+} in TNO-V are expected to be partially reduced into Ti^{3+} and/or Nb^{4+} by introducing oxygen vacancy. In addition, ionic radii for Ti^{3+} and Nb^{4+} are 67 pm and 68 pm, larger than those for Ti^{4+} (61 pm) and Nb^{5+} (64 pm). Slightly larger lattice parameters for TNO-V than those for TNO-A could be attributed to the presence of Ti^{3+} and Nb^{4+}

We also carried out X-ray photoelectron spectroscopy (XPS) analysis for both powder samples to confirm the chemical state of both Ti and Nb in TNO-A and TNO-V. The XPS characterizations obtained for both powder samples are shown in Figure 4. For calibration of measurement data, small amount of AB powders were mixed into both TNO-A and TNO-V in the analysis. As shown in Figure. 4(a), two peaks of Ti $2P_{1/2}$ and Ti $2P_{3/2}$ spectra in TNO-A are observed at binding energy around 465.3 and 459.7 eV, suggesting that the existence and occupying of Ti^{4+} in an octahedral environment.[35, 37, 38] These peaks are confirmed in TNO-V, but Ti $2P_{3/2}$ spectrum in TNO-V slightly shifts toward lower binding energy compared to TNO-A, indicating that small amounts of Ti^{4+} in TNO-V are reduced to Ti^{3+} caused by introduction of oxygen vacancy.[35, 40] In Figure. 4(b) for Nb 3d spectra, two peaks located at 208.1 eV for Nb $3d_{5/2}$ and 210.9 eV for Nb $3d_{3/2}$ are confirmed in TNO-A indicating the presence of Nb^{5+}.[35, 37, 38] These two peaks are also detected in TNO-V, but the peak shift toward lower binding energy due to the presence of Nb^{4+} caused by introduction of oxygen vacancy are quite small, so the presence of Nb^{4+} in V-TNO could not be characterized enough. For further examination,

the curve fitting for Ti $2P_{3/2}$ spectra for both TNO-A and TNO-V was carried out and the results are shown in Figure 4(c). The peaks for Ti^{3+} $2P_{3/2}$ and Ti^{4+} $2P_{3/2}$ are located around 458.8 and 459.7 eV.[9] and the contribution of Ti^{3+} becomes remarkable in TNO-V compared to TNO-A.

As previously reported, electronic conductivity for $Ti_2Nb_{10}O_{29-x}$ with oxygen vacancy is much higher than stoichiometric $Ti_2Nb_{10}O_{29}$, due to the presence of Ti^{3+} and/or Nb^{4+} in the crystal lattice.[38–40] In order to evaluate the influence of oxygen vacancy on electronic conductivity for $TiNb_2O_7$, potentiostatic polarization measurement at 30°C was carried out for TNO-A and TNO-V. Each powder sample with 0.3 g in weight was put between the pair of SUS316L electrode with cylindrical shape and then uni-axially pressed under applying pressure of 5×10^3 N. Applied DC voltage in the measurement was fixed to 1.0 V. Geometrical parameter of both pressed powder samples are 11 mm in diameter and 2 mm in thickness. DC polarization curves in both pressed TNO-A and TNO-V measuring electron conduction are shown in Figure. 5. Steady state current at 10 h after applying DC voltage are 4.5×10^{-8} mA for TNO-A and 5.1 mA for TNO-V, respectively. The electrical resistance R_e of each sample is calculated using the steady state current, applied DC voltage (= 1 V) and geometrical parameters of each sample. The electronic conductivity σ_e of pressed powder sample can be derived by using R_e and geometrical parameters as mentioned above. As a result, the electronic conductivity of pressed TNO-V was estimated to be 1.1×10^{-3} S cm^{-1}. On the other hand, the conductivity of pressed TNO-A was 0.95×10^{-11} S cm^{-1}, which is consistent with the reported value for air-annealed $TiNb_2O_7$ in the literatures.[33] This indicates that the electronic conductivity of TNO is increased by eight orders by introduction of oxygen vacancy.

Figure 5 is the comparison of initial charge (Li^+ insertion) and discharge (Li^+

extraction) profiles for TNO-A and TNO-V electrodes at 20°C and current density of 0.5 mA cm^{-2}. As shown in Figure 5, both TNO-A and TNO-V shows narrower voltage plateau around 1.8 V and wider plateau around 1.65 V, which is consistent with the results as previously reported.[26–35] It has been reported that in the potential range from 2.5 to 1.0 vs. Li/Li^+, Ti^{4+} in TNO is continuously reduced into Ti^{3+} and Nb^{5+} is also reduced into Nb^{4+} and sequentially reduced into Nb^{3+} from this potential range.[31, 32] Despite of the differences in the reversible capacities, the profiles for both cells are quite similar, indicating that the introduction of oxygen vacancy in TNO do not affect the fundamental electrochemical reaction mechanism. TNO-V with oxygen vacancy has slightly lower capacity than TNO-A. Initial charge and discharge capacities are 270.9 mAh g^{-1} and 267.3 mAh g^{-1} for TNO-A while 263.5 mAh g^{-1} and 259.8 mAh g^{-1} for TNO-V, respectively. It is known that all the electrochemical energy in TNO comes from the reversible redox reactions between Ti^{3+} and Ti^{4+} ions, between Nb^{4+} and Nb^{5+} ions, and between Nb^{3+} and Nb^{4+} ions. Since there are some amounts of Ti^{3+} and/or Nb^{4+} ions in TNO-V with oxygen vacancy, the contents of Ti^{4+} and/or Nb^{5+} become smaller than TNO-A without oxygen vacancy, leading to the lower reversible capacity at low current density. If the decrease of reversible capacity (= 7.6–7.7 mAh g^{-1}) in TNO-V at low current density (= 0.5 mA cm^{-2}) was caused by the partial reduction of Ti^{4+} and/or Nb^{5+} into Ti^{3+} and/or Nb^{4+}, oxygen content in TNO-V is estimated to be 6.90, which is close to the result (= 6.91) derived from TG measurement in Figure 3.

The charge–discharge curves of both TNO-A and TNO-V electrodes at 20°C and different fixed current densities per unit-electrode area of 1.0–5.0 mA cm^{-2} are shown in Figure 7. At current density of 1 mA cm^{-2}, both electrodes showed the reversible capacity around 250 mAh g^{-1}. The charge and discharge capacities for both electrodes are

decreased monotonically with increasing current densities, but TNO-V shows much smaller polarization and larger capacity than TNO-A under the current density above 2.0 mA cm^{-2}. This tendency becomes more significant as the current density is increased. At the highest current density of 5.0 mA cm^{-2}, TNO-V maintains the discharge capacity of 140 mAh g^{-1} while the capacity of TNO-A is limited to only 80 mAh g^{-1}. Such remarkable improvement of rate performance in TNO-V is mainly attributed to the enhancement of intrinsic electronic conductivity by introduction of oxygen vacancy.

Figure 8(a) shows the cycling performance for discharge capacities of TNO-A and TNO-V electrodes at 20°C and current density of 2.0 mA cm^{-2}. For direct comparison, the cycling performance for LTO electrode (70:25:5 (wt%) mixture of LTO as an active material, AB as a conducting additive and PTFE as a binder) with a thickness of 0.5 mm and a diameter of 8 mm, measured at same condition. Notably, LTO used in this measurement was prepared by a conventional solid state reaction, and its particle size is in the range from 0.5 to 1 μm (see inset of Figure 8(a)). As can be seen, both TNO-A and TNO-V electrode has higher capacities than LTO. Moreover, TNO-V electrode has higher capacity than TNO-A electrode in the whole cycles, suggesting that higher intrinsic electronic conductivity of the former than the latter is maintained during the cycling. The capacity retentions after 50 cycles for both TNO-A and TNO-V electrodes were around 90% and the coulombic efficiencies of both electrodes are nearly 100% during the whole cycle (Figure 8(b)). The results indicate that introduction of oxygen vacancy in TNO lattice and enhancement of intrinsic electronic conductivity has no notable influence on the cycling performance of TNO, and the cycling performance of active material is influenced by not only the intrinsic conductivity but also the magnitude of volume change during the electrode reaction. However, the cycling stability of both TNO-A and TNO-V

electrodes is inferior to LTO electrode with the capacity retention of 97% after 50 cycles. One of the main reason for lower cycling stability in TNO-A and TNO-V electrodes comparing to LTO electrode is expected to be the difference in volume change during Li^+ insertion/extraction reaction. It is well known that volume change in LTO during the Li^+ insertion/extraction reaction is negligibly small (< 0.2%),[5] while it has been confirmed that larger volume change (~8%) occurs in TNO during the Li^+ insertion/extraction reaction at an electrical potential above 1 V vs. Li/Li^+.[31, 32] This would cause the mechanical damages in active material and promote the degradation of electrochemical performance with cycling.

4. CONCLUSION

We investigated the properties for $TiNb_2O_7$ (TNO) annealed in air (TNO-A) or vacuum (TNO-V) as high potential anode material for LiB. Oxygen vacancy is easily introduced in TNO lattice by vacuum annealing for precursor materials for TNO. XPS analysis also indicated that Ti^{4+} in TNO-V are partially reduced into Ti^{3+} due to the introduction of oxygen vacancy. Room temperature electronic conductivity for uni-axially pressed TNO-V powder is estimated to be around 10^{-3} S cm^{-1}, which is eight orders higher than that for pressed TNO-A powder. In electrochemical testing, both TNO-A and TNO-V electrodes showed reversible capacity of 260–270 mAh g^{-1} at low current density, but at higher current density, TNO-V electrode showed much higher capacity than that for TNO-A. The improvement in rate performance for TNO-V is mainly attributed to the enhancement of intrinsic electronic conductivity.

ACKNOWLEDGEMENTS

This work was partly supported by Research Grants from The Hibi Science Foundation.

REFERENCES

1. Tarascon JM, Armand M. Issues and challenges facing rechargeable lithium batteries. Nature. 2011; 414:359–367.
2. Scrosati B, Garche J. Lithium batteries: status, prospects and future. J Power Sources. 2010; 195:2419–2430.
3. Goodenough JB, Kim Y. Challenges for rechargeable batteries. J Power Sources. 2011; 196:6688–6694.
4. Chen Z, Belharouak I, Sun YK, Amine K. Titanium-based anode materials for safe lithium-ion batteries. Adv Funct Mater. 2013; 23:959–969.
5. Ohzuku T, Ueda A, Yamamoto N. Zero-strain insertion material of $Li[Li_{1/3}Ti_{5/3}]O_4$ for rechargeable lithium cells. J Electrochem Soc. 1995; 142:1431−1435.
6. Yoshikawa D, Kadoma Y, Kim JM, Ui K, Kumagai N, Kitamura N, et al. Spray-drying synthesized lithium-excess $Li_{4+x}Ti_{5-x}O_{12-\delta}$ and its electrochemical property as negative electrode material for Li-ion batteries. Electrochimica Acta. 2010; 55:1872−1879.
7. Song MS, Benayad A, Choi YM, Park KS. Does $Li_4Ti_5O_{12}$ need Carbon in lithium ion batteries? Carbon-free electrode with exceptionally high electrode capacity. Chem Commun. 2011; 48:516–518.
8. Wolfenstine J, Allen JL. Electrical conductivity and charge compensation in Ta doped $Li_4Ti_5O_{12}$. J Power Sources. 2008; 180:582−585.
9. Yu Z, Zhang X, Yang G, Liu J, Wang J, Wang R, et al. High rate capability and long-

term cyclability of $Li_4Ti_{4.9}V_{0.1}O_{12}$ as anode material in lithium ion battery. Electrochimica Acta. 2011; 56:8611–8617.

10. Zhang Q, Zhang C, Li B, Jiang D, Kang S, Li X, et al. Preparation and characterization of W-doped $Li_4Ti_5O_{12}$ anode material for enhancing the high rate performance. Electrochimica Acta. 2013; 107:139–146.
11. Song H, Jeong TG, Moon YH, Chun HH, Chung KW, Kim HS, et al. Stabilization of oxygen-deficient structure for conducting $Li_4Ti_5O_{12-\delta}$ by molybdenum doping in a reducing atmosphere. Scientific Reports. 2014; 4:4350.
12. Inaba M, Oba T, Niina F, Murota Y, Ogino Y, Tasaka A, et al. TiO_2(B) as a promising high potential negative electrode for large-size lithium-ion batteries. J Power Sources. 2009; 189:580–584.
13. Ren Y, Liu Z, Pourpoint F, Armstrong AR, Grey CP, Bruce PG. Nanoparticulate TiO_2(B): an anode for lithium-ion batteries. Angew Chem. 2012; 124:2206–2209.
14. Saito M, Nakano Y, Takagi M, Honda N, Tasaka A, Inaba M. Improvement of tap density of TiO_2(B) powder as high potential negative electrode for lithium ion batteries. J Power Sources. 2013; 244:50–55.
15. Kuhn A, Amandi R, Garcia-Alvarado F. Electrochemical lithium insertion in TiO_2 with the ramsdellite structure. J Power Sources. 2001; 92:221–227.
16. Villevielle C, Van Thournout M, Scoyer J, Tessier C, Olivier-Fourcade J, Jumas JC, et al. Carbon modified $Li_2Ti_3O_7$ ramsdellite electrode for Li-ion batteries. Electrochimica Acta. 2010; 55:7080–7084.
17. Setiawati E, Hayashi M, Takahashi M, Shodai T, Saito K. Effect of annealing on the electrochemical properties of ramsdellite-type lithium titanium oxide. J Power Sources. 2011; 196:10133–10140.

18. Akimoto J, Kataoka K, Kojima N, Hayashi S, Gotoh Y, Sotokawa T, et al. A novel soft-chemical synthetic route using $Na_2Ti_6O_{13}$ as a starting compound and electrochemical properties of $H_2Ti_{12}O_{25}$. J Power Sources. 2013; 244:679–683.
19. Cava RJ, Murphy DW, Zahurak SM. Lithium insertion in Wadsley-Roth phases based on niobium oxide. J Electrochem Soc. 1983; 130:2345–2451.
20. Le Vieta A, Reddya MV, Joseb R, Chowdaria BVR, Ramakrishna S. Electrochemical properties of bare and Ta-substituted Nb_2O_5 nanostructures. Electrochimica Acta. 2011; 56:1518–1528.
21. Sasidharan M, Gunawardhana N, Yoshio M, Nakashima K. Nb_2O_5 hollow nanospheres as anode material for enhanced performance in lithium ion batteries. Mater Res Bull. 2012; 47:2161–2164.
22. Pralong V, Reddy MA, Caignaert V, Malo S, Lebedev OI, Varadaraju UV, et al. A new form of $LiNbO_3$ with a lamellar structure showing reversible lithium intercalation. Chem Mater. 2011; 23:1915–1922.
23. Jian Z, Lu X, Fang Z, Hu YS, Zhou J, Chen W, et al. $LiNb_3O_8$ as a novel anode material for lithium-ion batteries. Electrochem Commun. 2011; 13:1127–1130.
24. Saritha D, Pralong V, Varadaraju UV, Raveau B. Electrochemical Li insertion studies on $WNb_{12}O_{33}$ - a shear ReO_3 type structure. J Solid State Chem. 2010; 183:988–993.
25. Colin JF, Pralong V, Hervieu M, Caignaert V, Raveau B. Lithium insertion in an oriented nanoporous oxide with a tunnel structure: $Ti_2Nb_2O_9$. Chem Mater. 2008; 20:1534–1540.
26. Han JT, Huang YJ, Goodenough JB. New anode framework for rechargeable lithium batteries. Chem Mater. 2011; 23:2027–2029.
27. Han JT, Goodenough JB. 3-V full cell performance of anode framework

$TiNb_2O_7$/Spinel $LiNi_{0.5}Mn_{1.5}O_4$. Chem Mater. 2011; 23:3404–3407.

28. Lu Z, Jian Z, Fang Z, Gu L, Hu YS, Chen W, et al. Atomic-scale investigation on lithium storage mechanism in $TiNb_2O_7$. Energy Environ Sci. 2011; 4:2638–2644.
29. Tang K, Mu XK, Aken PW, Yu Y, Maier J. "Nano-pearl-string" $TiNb_2O_7$ as anodes for rechargeable lithium batteries. Adv Energy Mater. 2012; 3:49–53.
30. Jayaraman S, Aravindan V, Kumar PS, Ling WC, Ramakrishna S, Madhavi S. Exceptional performance of $TiNb_2O_7$ anode in all one-dimensional architecture by electrospinning. ACS Appl Mater Interfaces. 2014; 6:8660–8666.
31. Guo B, Yu X, Sun XG, Chi M, Qiao ZA, Liu J, et al. A long-life lithium-ion battery with a highly porous $TiNb_2O_7$ anode for large-scale electrical energy storage. Energy Environ Sci. 2014; 7:2220–2226.
32. Ise K, Morimoto S, Harada Y, Takami N. Large lithium storage in highly crystalline $TiNb_2O_7$ nanoparticles synthesized by a hydrothermal method as anodes for lithium-ion batteries. Solid State Ionics. 2018; 320:7–15.
33. Yang C, Lin C, Lin S, Chen Y, Li J. $Cu_{0.02}Ti_{0.94}Nb_{2.04}O_7$: an advanced anode material for lithium-ion batteries of electric vehicles. J Power Sources. 2016; 328:336–344.
34. Lin S, Yu S, Wu S, Lin S, Zhu ZZ, Lia J, et al. $Ru_{0.01}Ti_{0.99}Nb_2O_7$ as an intercalation-type anode material with a large capacity and high rate performance for lithium-ion batteries. J Mater Chem A. 2015; 3:8627–8635.
35. Song H, Kim YT. A Mo-doped $TiNb_2O_7$ anode for lithium-ion batteries with high rate capability due to charge redistribution. Chem Commun. 2015; 51:9849–9852
36. Wu X, Myao J, Han W, Yu YS, Chen D, Lee JS, et al. Investigation on $Ti_2Nb_{10}O_{29}$ anode material for lithium-ion batteries. Electrochem Commun. 2012; 25:39–42.
37. Yang C, Yu S, Ma Y, Lin C, Xu Z, Zhao H, et al. Cr^{3+} and Nb^{5+} co-doped $Ti_2Nb_{10}O_{29}$

materials for high-performance lithium-ion storage. J Power Sources. 2017; 360:470–479.

38. Takashima T, Tojo T, Inada R, Sakurai Y. Characterization of mixed titanium–niobium oxide $Ti_2Nb_{10}O_{29}$ annealed in vacuum as anode material for lithium-ion battery. J Power Sources. 2015; 276:113–119.
39. Lin CF, Yu S, Zhao H, Wu SQ, Wang GZ, Yu L, et al. Defective $Ti_2Nb_{10}O_{27.1}$: an advanced anode material for lithium-ion batteries. Scientific Reports. 2015; 5:17836.
40. Deng S, Luo Z, Liu Y, Lou X, Lin C, Yang C, et al. $Ti_2Nb_{10}O_{29-x}$ mesoporous microspheres as promising anode materials for high-performance lithium-ion batteries. J Power Sources. 2017; 362:250–257.
41. Yang C, Deng S, Lin C, Lin S, Chen Y, Li J, et al. Porous $TiNb_{24}O_{62}$ microspheres as high-performance anode materials for lithium-ion batteries of electric vehicles. Nanoscale. 2016; 8:18792–18799.
42. Li R, Qin Y, Liu X, Yang L, Lin C, Xia R, et al. Conductive $Nb_{25}O_{62}$ and $Nb_{12}O_{29}$ anode materials for use in high-performance lithium-ion storage. Electrochimica Acta. 2018; 266:202–211.

FIGURE CAPTIONS

FIGURE 1. (a) Comparison of X-ray diffraction patterns for TNO-A annealed in air and TNO-V annealed in vacuum. An inset is the crystal structure of $TiNb_2O_7$ along *ac*-plane. Enlarged several specific diffraction peaks for both samples are shown in (b).

FIGURE 2. Photos (left) and SEM images (right) for TNO-A annealed in air (a) and TNO-V annealed in vacuum (b).

FIGURE 3. Comparison of thermogravimetric (TG) curves for TNO-A and TNO-V. The measurement was carried out in flowing air with 500 mL min^{-1}.

FIGURE 4. Comparison for Ti 2p (a) and Nb 3d (b) spectrum for TNO-A and TNO-V measured by X-ray photoelectron spectroscopy. Fitting results (solid lines) for Ti 2p 2/3 spectrum for TNO-A and TNO-V are shown in (c).

FIGURE 5. DC polarization curves in pressed TNO-A and TNO-V measuring electron conduction at 1 V and 30°C.

FIGURE 6. Comparison of initial charge (Li^+ insertion) and discharge (Li^+ extraction) curves at 20°C and current density of 0.5 mA cm^{-2} for TNO-A (dashed line) and TNO-V (solid line) electrodes.

FIGURE 7. Charge (solid lines) and discharge (dashed lines) curves at 20°C and different fixed charge and discharge current densities from 1.0 to 5.0 mA cm^{-2} for (a) TNO-A and (b) TNO-V electrodes.

FIGURE 8. (a) Discharge capacities for TNO-A, TNO-V and LTO electrodes at constant current density of 2.0 mA cm^{-2} at 20°C plotted against cycle numbers. The inset SEM image of LTO particles used in this measurement. Coulombic efficiencies of both TNO-A and TNO-V electrodes are also plotted as a function of cycle numbers in (b).

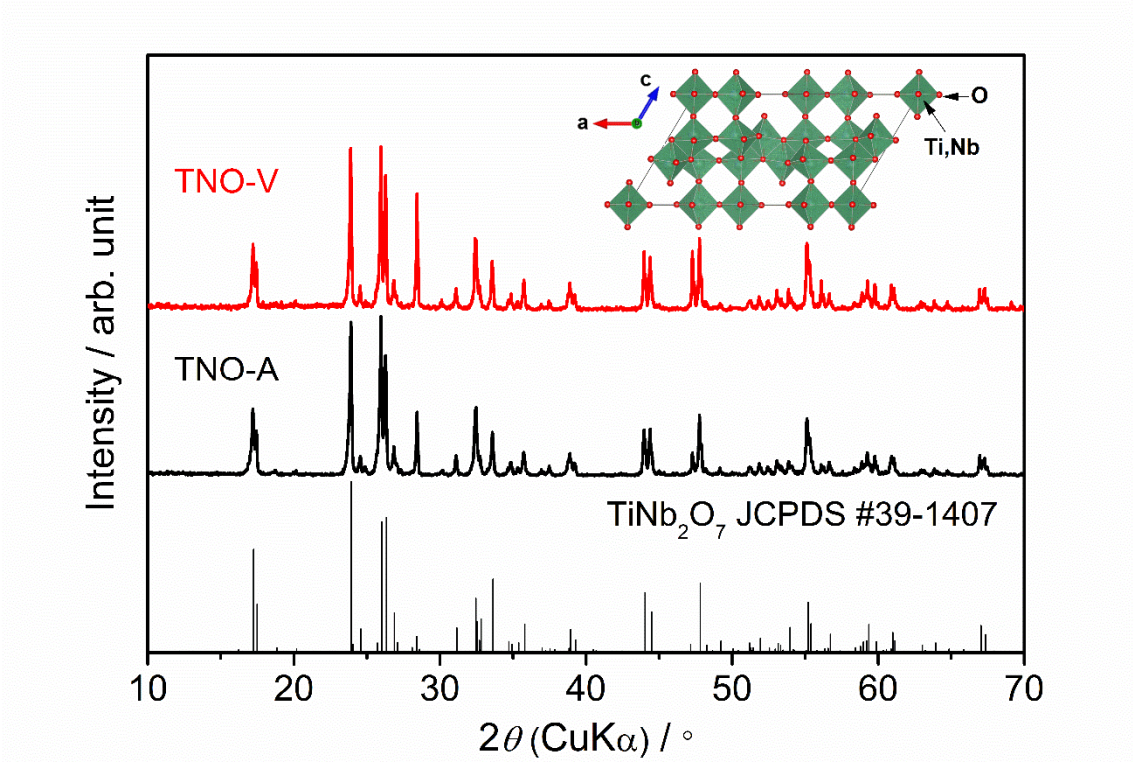

Figure 1(a)

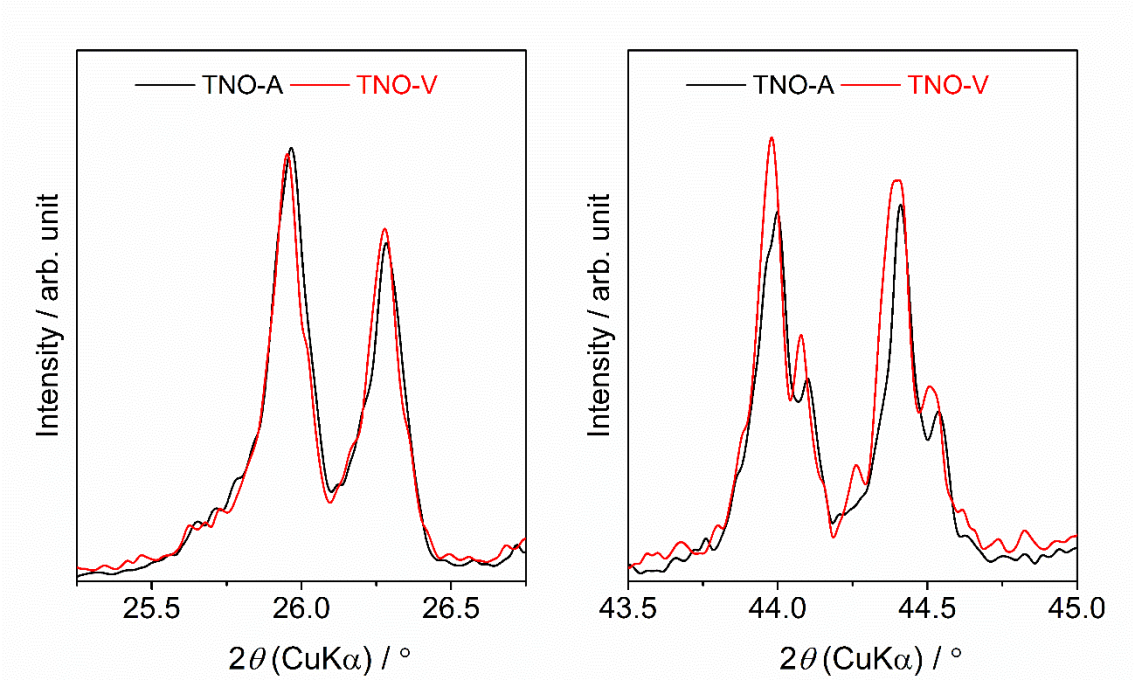

Figure 1(b)

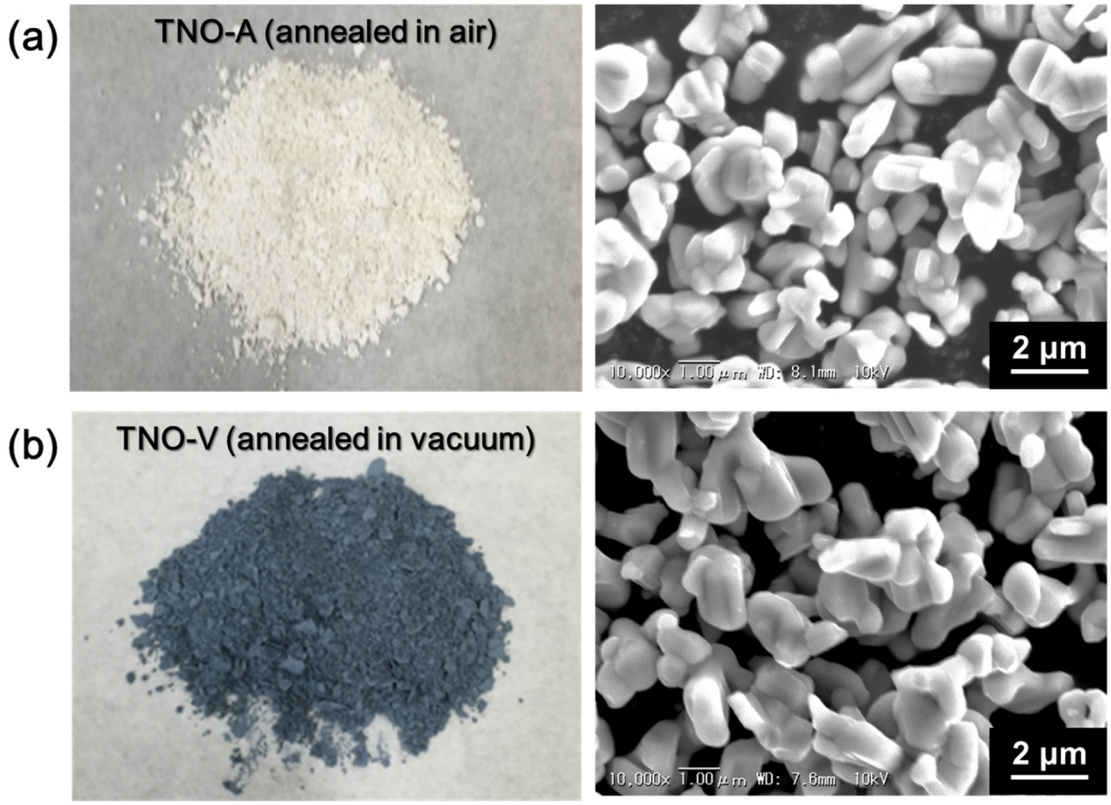

Figure 2

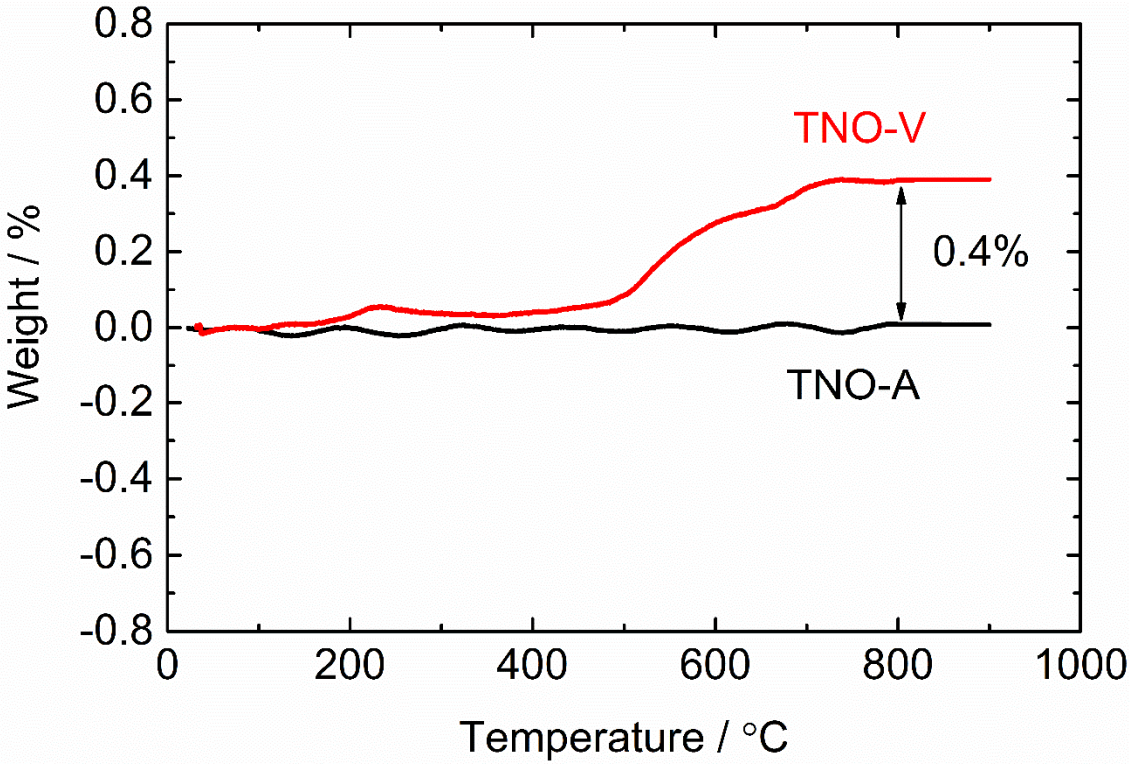

Figure 3

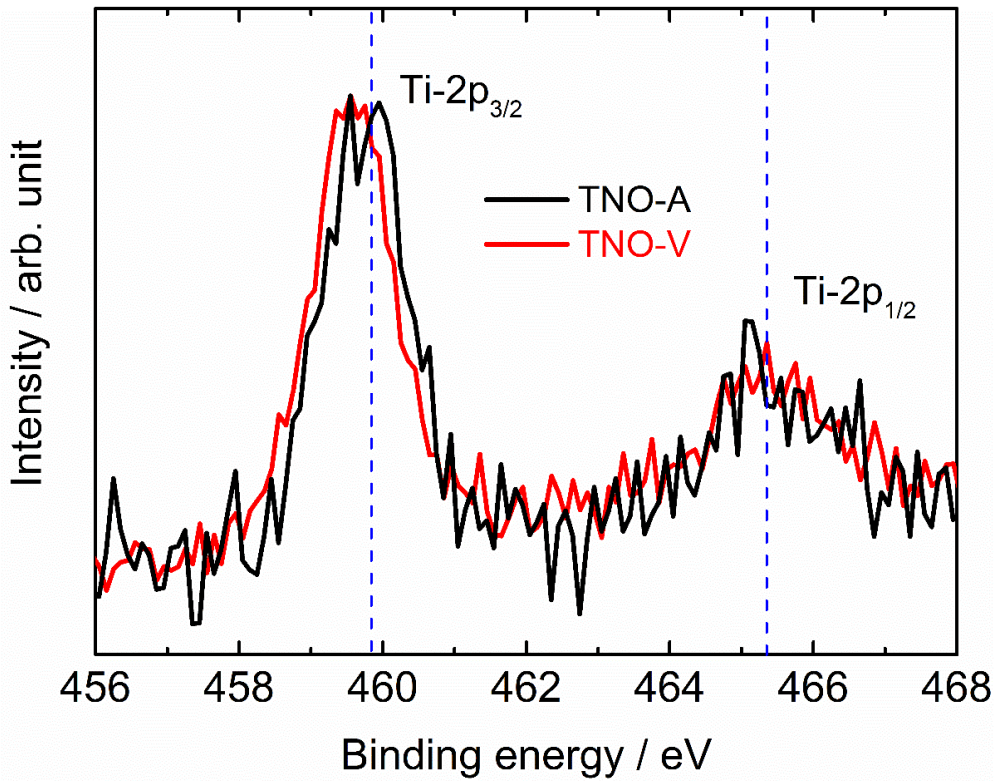

Figure 4(a)

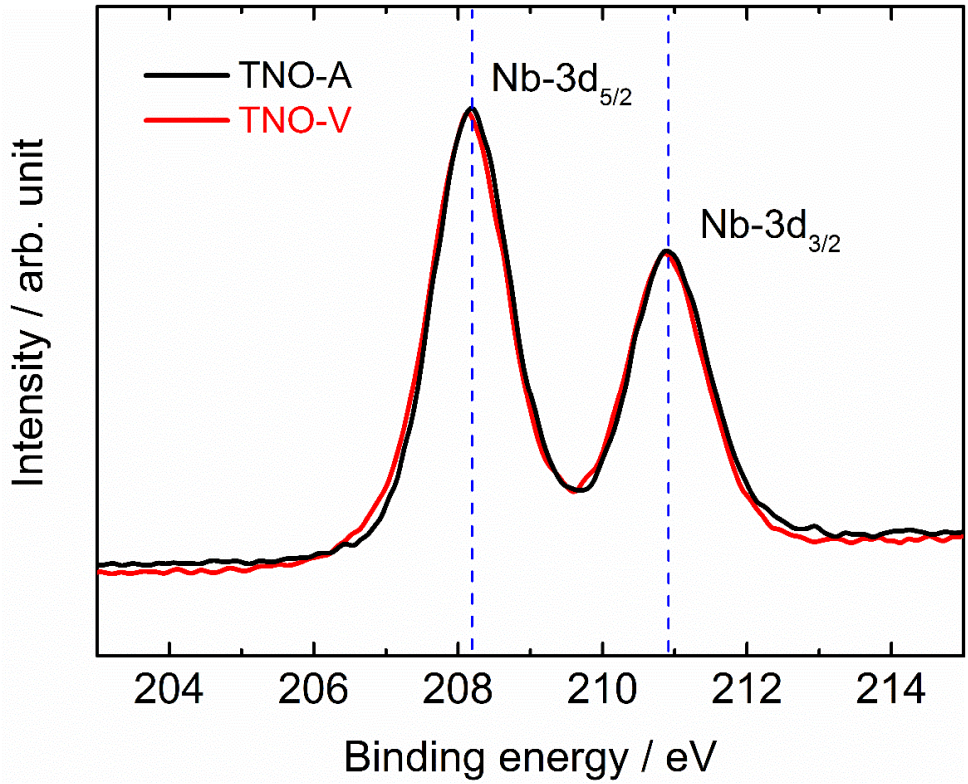

Figure 4(b)

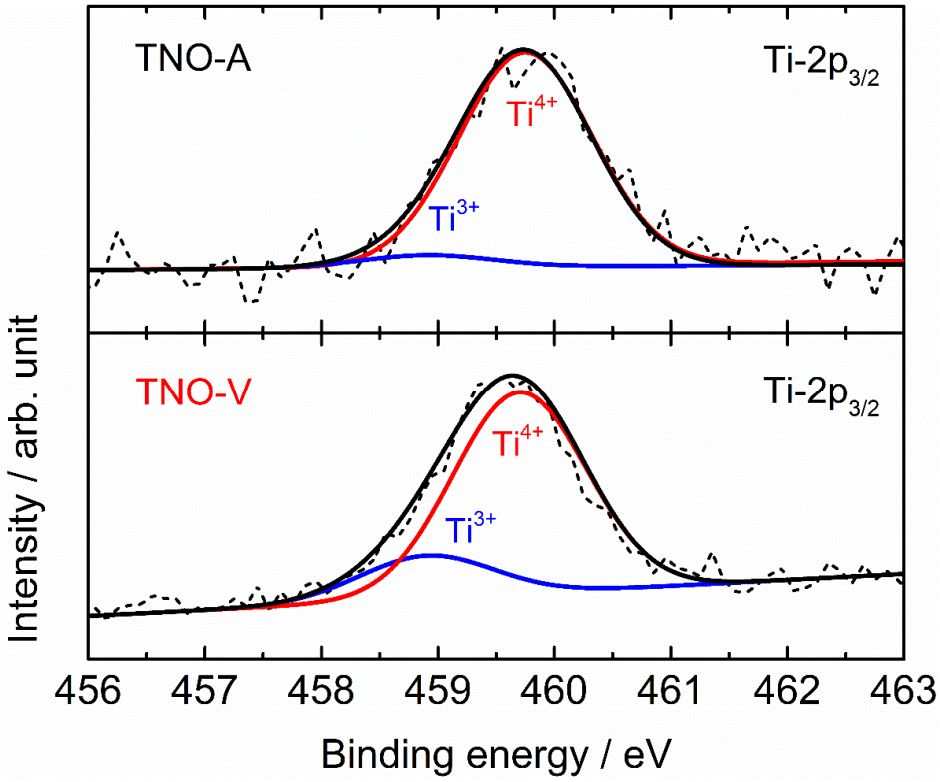

Figure 4(c)

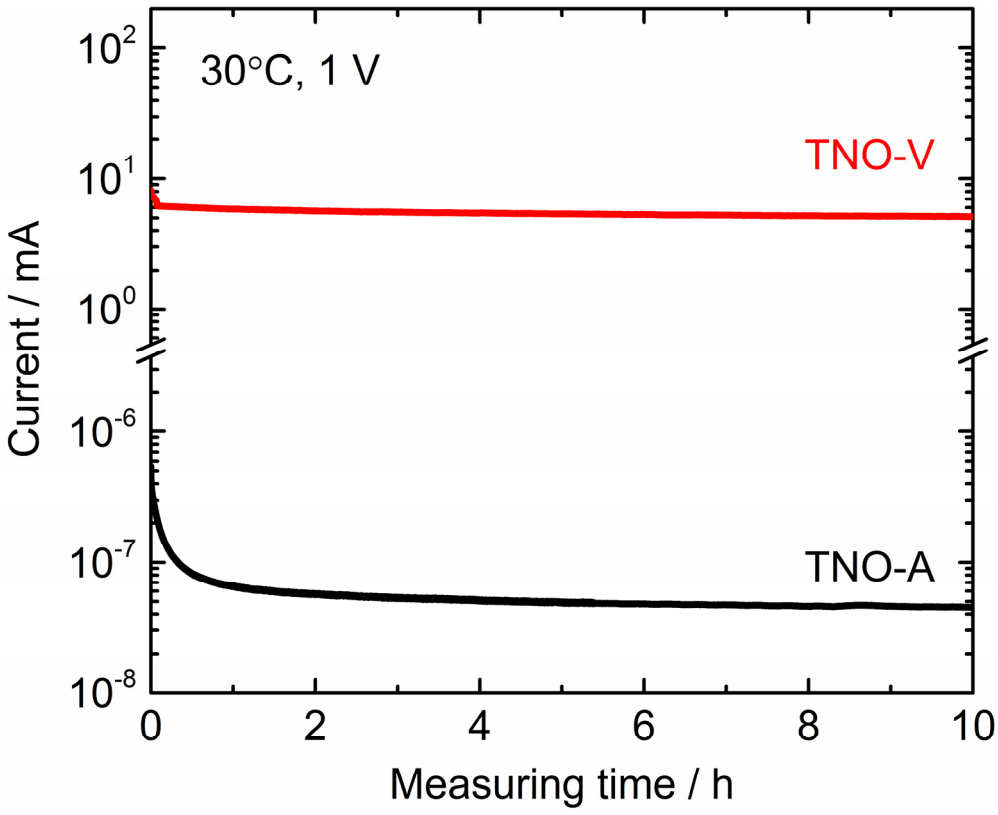

Figure 5

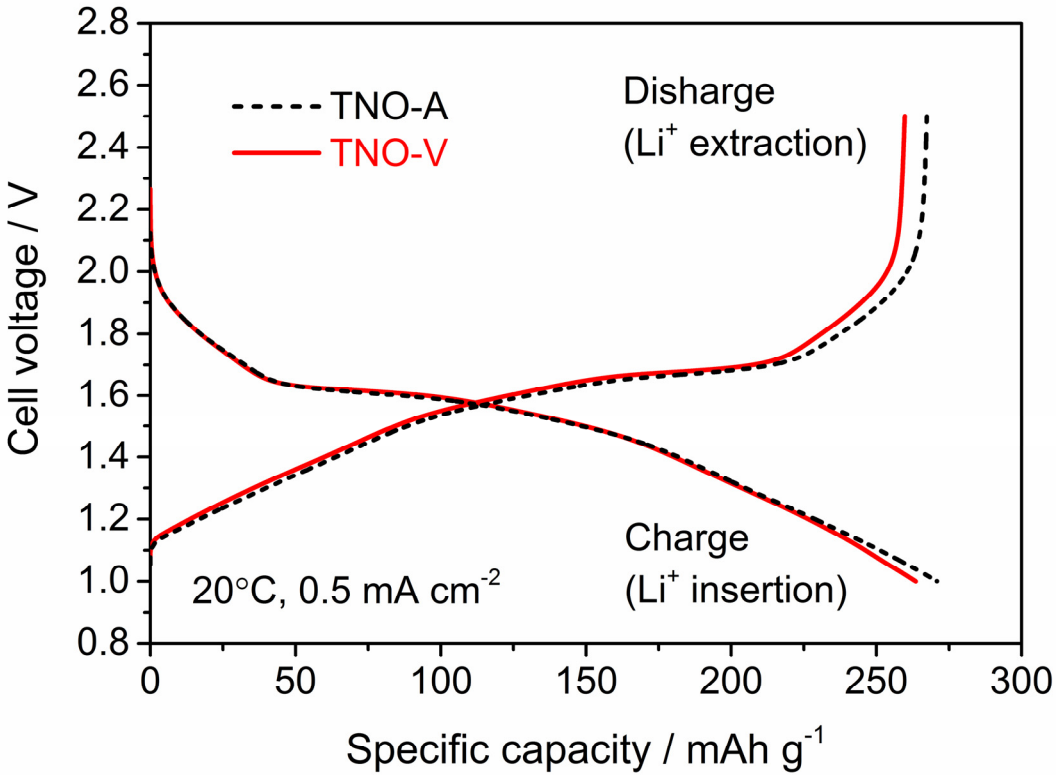

Figure 6

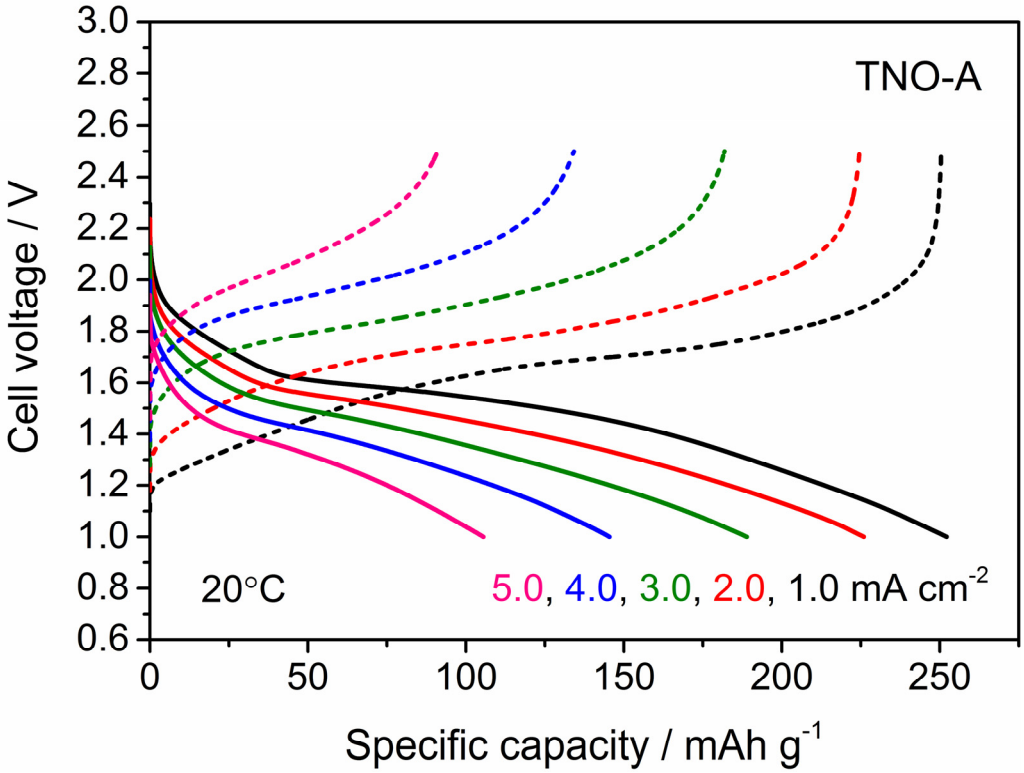

Figure 7(a)

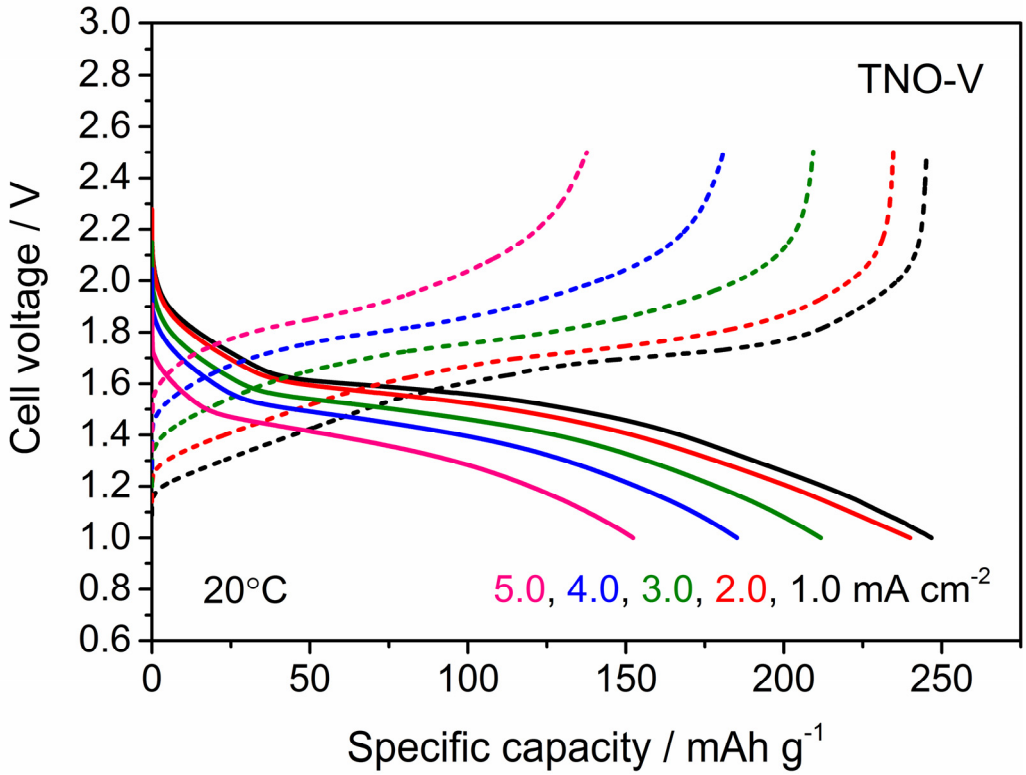

Figure 7(b)

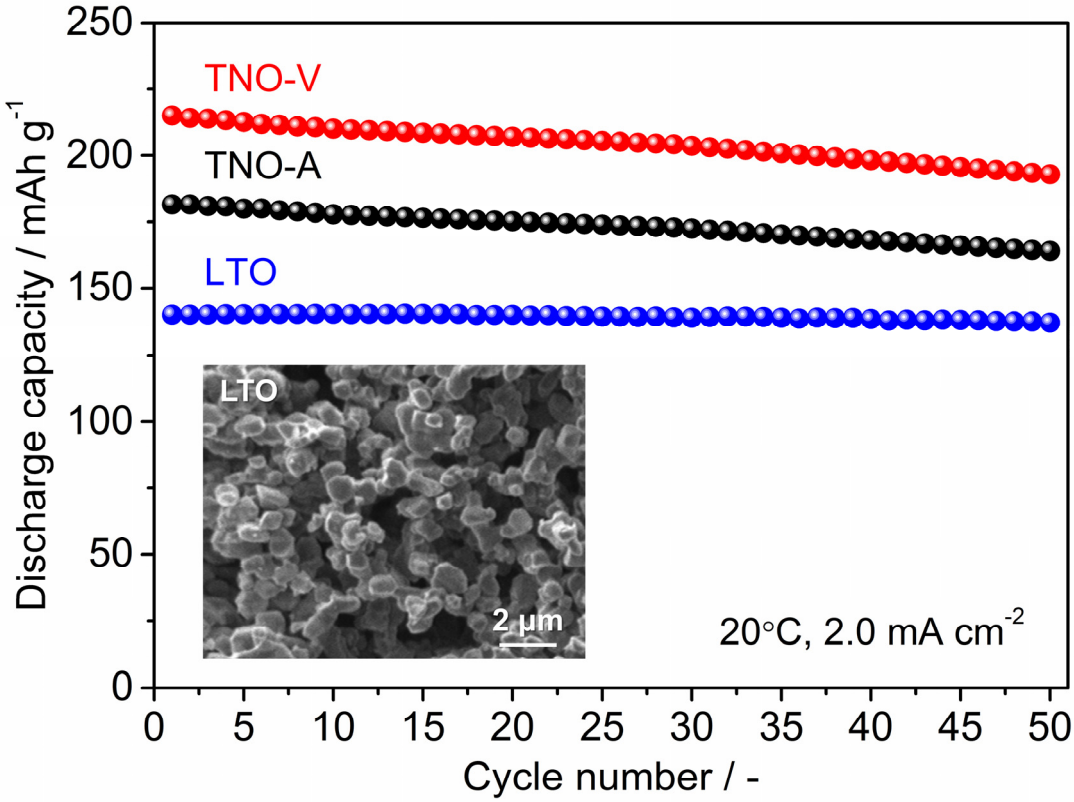

Figure 8(a)

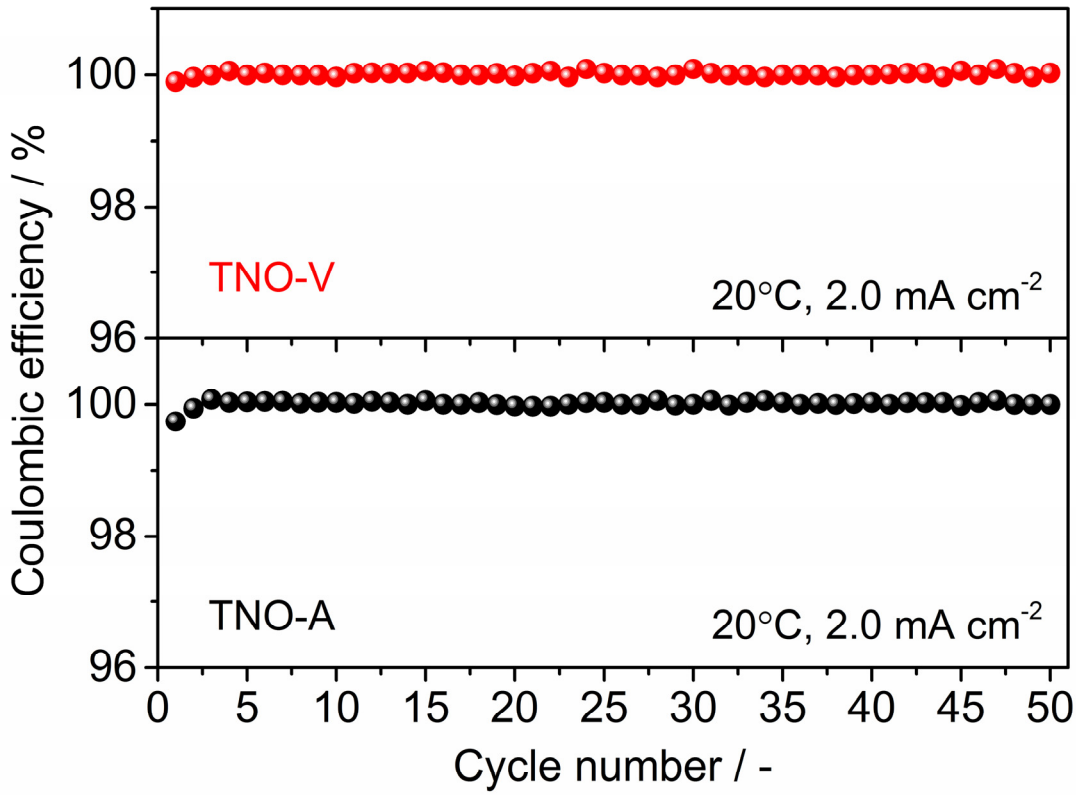
Coulombic efficiency / %
100
98
96
TNO-V
20°C, 2.0 mA cm-2
100
98
96
TNO-A
20°C, 2.0 mA cm-2
0
5
10
15
20
25
30
35
40
45
50
Cycle number / -

Figure 8(b)